SPANDIDOS PUBLICATIONS

INTERNATIONAL JOURNAL OF ONCOLOGY 61: 133, 2022

Isolation and analysis of tumor-derived extracellular vesicles from head and neck squamous cell carcinoma plasma by galectin-based glycan recognition particles

LAURA BENECKE[1,2*], DAPI MENGLIN CHIANG[1,3,4*], ELIANE EBNOETHER[1,2], MICHAEL W. PFAFFL[3] and LAURENT MULLER[1,2]

[1]Department of Biomedicine, University of Basel; [2]Department of Otorhinolaryngology, Head and Neck Surgery, University Hospital of Basel, 4031 Basel, Switzerland; [3]Department of Animal Physiology and Immunology, School of Life Sciences, Technical University Munich, D-85354 Freising, Germany; [4]Biovesicle Inc., Taipei 10047, Taiwan, R.O.C.

Received February 22, 2022; Accepted July 15, 2022

DOI: 10.3892/ijo.2022.5423

Abstract. Extracellular vesicles (EVs) have recently come into the spotlight as potential cancer biomarkers. Isolation of pure EVs is complex, so wider use requires reliable and time-efficient isolation methods. In the present study, galectin-based magnetic glycan recognition particles, EXÖBead® were investigated for their practicality as a novel EV isolation technique, exemplified here for squamous cell carcinoma of the head and neck. Analysis of the isolation method showed a high concentration of pure EVs with detection of specific EV markers such as CD9, CD63, CD81 and TSG101. No apolipoprotein A1 was shown in the isolates, indicating low contamination of this isolation technique compared with size exclusion chromatography. In addition, common leukocyte antigen (CD45), three HNSCC [epithelial cell adhesion molecule (EpCAM), pan-cytokeratin and programmed death-ligand 1 (PD-L1)] and PanEV markers (premixed CD9, CD63 and CD81 antibodies) were measured by bead-based flow cytometry (BFC). BFC revealed that $CD45^{Neg}$ $PanEV^{+}$, $EpCAM^{+}$ $PanEV^{+}$ and $PD\text{-}L1^{+}$ $PanEV^{+}$ were significantly higher in tumor patients compared with healthy control plasma. $CD45^{Neg}$ $PanEV^{+}$ and $CD45^{+}$ $PanEV^{+}$ carrying two or three HNSCC biomarkers were also significantly higher in tumor patients compared with healthy controls (BFC). Comparison of the functional immunosuppression effect of eluted tumor patient plasma EVs from EXÖBead® and commercial polyethylene glycol isolation showed a significant tumor-dependent increase in concentration of EVs. A peripheral blood mononuclear cell activation assay also showed that the T-cell functionality of tumor patient plasma EVs isolated with EXÖBead® was preserved *in vitro*. In conclusion, isolation using galectin-based magnetic glycan recognition particles is a novel method for isolating plasma EVs with low lipoprotein contamination. Bead-based flow cytometry provided an easy way to understand EV subpopulations. EXÖBead® therefore showed great potential as a new isolation tool with high throughput capacity that could potentially be used in a clinical setting.

Correspondence to: Dr Laurent Muller, Department of Biomedicine, University of Basel, Hebelstrasse 20, 4031 Basel, Switzerland
E-mail: laurent.muller@usb.ch

*Contributed equally

Key words: extracellular vesicles, exosomes, novel isolation technique, biomarker, head and neck squamous cell carcinoma, tumor-derived extracellular vesicles, galectin-based glycan recognition particles, beads-based flow cytometry

Introduction

Several decades have passed since the first discovery and scientific description of EVs in 1983 as 'blebbling of membranes'. Research in the following years showed that they participate in intercellular communication and molecule exchange. Cancer cells are also considered to make extensive use of this novel form of vesicular communication. Therefore, EVs have become the focus of interest in recent years as potential biomarkers for cancer diagnosis, cancer progression, disease monitoring and response to chemotherapeutic agents (1,2). EVs are produced in large numbers by cancer cells, named tumor-derived EVs, implicating a possible explanation for tumor spread and induction of the immunosuppressive tumor microenvironment (3). Furthermore, several studies have demonstrated the immunosuppressive nature of tumor EVs including EVs derived from squamous cell carcinoma (4).

Head and neck squamous cell carcinoma (HNSCC) is the 6th most frequent cancer worldwide. Globally, 666,037 cases were reported in 2018 (5). Although great progress has been made in diagnosis and treatment, the 5-year overall survival rate remains poor at 60% and even worse in the more advanced stages. Half of the patients with an advanced HNSCC suffer a recurrence within two years (6). The current standard diagnostic approach (endoscopy with at times invasive biopsies and imaging) requires vast medical experience, usually only available at medical centers, and thus often leads to delayed

diagnosis. Therefore, there is an urgent need for additional parameters in diagnostics and follow-up screening. As a consequence, nanoscale vesicles containing certain HNSCC proteins were investigated as potential circulating biomarkers (7-9). As previously described, EVs can be isolated in a large number in patients suffering from head and neck cancer (10,11).

Standard methods for EV isolation, such as ultra-centrifugation (UC), size exclusion chromatography (SEC), or affinity-based methods remain relatively time-consuming, susceptible for disturbance and difficult to implement into clinical setting (1,7,12,13) Consequently, there is a need for a more efficient, reliable EV isolation method that can be easily applied in clinical routine and yield purified EVs with low contamination. Progress to improve current isolation techniques has already been made by implementing columns and refinements (7-9,14).

In the present study, the potential clinical application of galectin-based glycan recognition particles (EXÖBead®) were investigated to isolate EVs from the blood of cancer patients. Previously, this technique was studied in patients with vascular problems and it was revealed that the functions of EVs were altered when treated with antihypertensive drugs (15). Our aim was to investigate a new and simplified isolation technique that eliminates the need for laborious ultracentrifugation and that can detect common EV markers. It was also investigated whether EVs eluted from EXÖBead® still displayed the familiar EV morphology. The clinical focus was on the isolation of EVs from the plasma of patients with HNSCC, their subtyping using various biomarkers and investigating their ability to immunosuppress. In the medium and long term, in addition to an improved understanding of the role of EVs in tumors, our investigations are intended to allow earlier detection of initial diagnoses and recurrences.

Materials and methods

Patient sample collection. Patients (n=18) from the department of otorhinolaryngology of the University hospital of Basel (Switzerland) with HNSCC in early and advanced stages were included as well as 3 healthy controls (Table I). The categorization is based on the current TNM 8 (16). The classification is used to divide malignant tumors into stages. The three main categories of the TNM system correspond to the three letters: T=tumor, extent and behavior of the primary tumor; N=nodus-absence or presence of regional lymph node metastases; M=metastases, absence or presence of distant metastases. Depending on this, a distinction is made between low grade and high grade (WHO I + II vs. III + IV). Ethical approval (approval no. 2020-02173) was issued by ethical commission of the northwest and central Switzerland. All patients provided written informed consent for research and consented to anonymous processing of the blood samples collected for scientific purposes. Blood collection was performed before the start of tumor therapy. A standardized peripheral venous blood collection of 7.5 ml blood was performed (EDTA; S-Monovette; Sarstedt). To remove cells and cell debris, whole blood was further centrifuged at 800 g, 10 min at room temperature. Platelet-rich plasma (PRP) was collected into new tubes. Platelet-poor plasma (PPP) was generated from PRP by additional 10,000 g centrifugation at 4˚C for 30 min, aliquoted and stored at -80˚C (7,12).

Galectin-based glycan recognition particles EVs isolation, EXÖBead®. The EXÖBead® used are magnetic beads coated with galectins for the isolation of EVs. The basis of this was the detection of N-linked glycoproteins on EVs, in particular galectin-3-binding protein (LGALS3BP), which was found on EVs from ovarian cancer cells (17-19).

PPP (1 ml) was diluted directly in 0.9 ml of 0.5% EV-free BSA (SERVA Electrophoresis GmbH) in PBS (100,000 g, 4˚C for overnight centrifugation) and incubated with 100 μl of EXÖBead® (1 μm, 6x10^8 particles/ml, Biovesicle Inc.) for 1 h at 25˚C. EV-EXÖBead® complexes were washed twice with 1 ml 0.5% EV-free BSA in PBS while magnetic EXÖBead® were kept in the tube by using a magnet (Biovesicle, Inc.). A total of 1 ml of 10% EV-free BSA in PBS was also incubated with EXÖBead® as a negative control (EF-EXÖBead® complex). Unbound plasma was also collected as the non-EVs fraction. Non-EVs fractions were further used in intracellular EV marker and non-EVs marker staining. EVs-EXÖBead® complexes and EF-EXÖBead® complex were further analyzed regarding EV surface marker, intracellular EV marker and non-EV marker staining. To dissolve EVs from the beads, EVs-EXÖBead® complexes were incubated with 200 μl of 0.3 M lactose in PBS with EV-EXÖBead® complexes at room temperature for 1 h. EF-EXÖBead® complex was also incubated with 0.3 M lactose in PBS as an elution buffer negative control. Particles from EF-EXÖBead® complex were too low to detect (data not shown). Eluted EVs were further analyzed by nanoparticle Tracking Analysis (NTA), transmission electron microscopy (TEM), cryogenic TEM (cryo-TEM) and peripheral blood mononuclear cells (PBMCs) functional assay (Fig. 1).

EVs surface marker staining. Antibody master mix (200 μl) was incubated each with plasma EV-EXÖBead® complexes as well as with EV-free (EF)-EXÖBead® complexes (1 ml of 10% EV-free BSA in PBS). Incubation lasted for 1 h at 25˚C. After antibody incubation, the EV-EXÖBead® and EF-EXÖBead® complexes were washed twice with 1 ml of 0.5% EV-free BSA in PBS, while the magnetic EXÖBead® were held in the tube using a magnet (Biovesicle, Inc.). Plasma EV-EXÖBead® and EF-EXÖBead® complexes stained with antibodies were subsequently prepared on the BD LSR Fortessa™ (BD Biosciences) and the data were analyzed using FlowJo software (Tree Star, Inc.). EF-EXÖBead® complexes served as a non-EV control. Plasma EV-EXÖBead® complexes were also stained with IgG antibodies. The background signal of EF-EXÖBead® complexes with test master mix antibodies and plasma EVs-EXÖBead® complexes with IgG antibodies was comparable (data not shown). EF-EXÖBead® complexes were used as the gating basis of the flow cytometry data. Our antibody master mix contained: 2.5 μg/ml of PE/Cyanine7 anti-human CD63 (1:80; clone: H5C6), FITC anti-human CD81 (1:80; clone: 5A6), APC anti-human CD9 (1:80; clone: HI9a; all from Biolegend, Inc.) and eFluor 450 anti-human programmed death-ligand 1 (PD-L1; 1:80; clone: MIH1; Thermo Fisher Scientific, Inc.). For the EV subpopulation gating strategy, $CD9^{+\text{ or Neg}}$ and $CD81^{+\text{or Neg}}$ were first gated on Plasma EV-EXÖBead® complexes which based on the background signal from EF-EXÖBead® complexes. These four-population included $CD9^+$ $CD81^{Neg}$, $CD9^+$ $CD81^+$, $CD9^{Neg}$ $CD81^+$ and $CD9^{Neg}$ $CD81^{Neg}$ plasma EV-EXÖBead® complexes.

Table I. Age and sex distribution of the samples. The samples were collected between June 2019 and March 2021.

Characteristics	Total (n=18)
Sex	
Male	13 (72.2%)
Female	5 (27,8%)
Age, years	
Mean (range)	68.9 (52-90)
≥65	9 (50%)
>65	9 (50%)

These four populations were further gated with $CD63^{+ \text{ or } Neg}$ and $PD\text{-}L1^{+ \text{ or } Neg}$ based on the signal of EF-EXÖBead® complexes. Significance was calculated by two-way ANOVA with Šídák's multiple comparisons test.

HNSCC biomarkers staining. Due to limited fluorescence channels, the PanEV antibody was used as a positive EV marker instead of three individual antibodies. PanEV antibody (3 μl) was premixed with 1 μl of PE anti-CD63: H5C6 clone, 1 μl of PE-CD81: 5A6 clone and 1 μl of PE-CD9: HI9a clone (1:66.7; Biolegend, Inc.). The antibody master mix contained the PanEV marker, three disease-specific biomarkers, and a common leukocyte antigen CD45. The mix was set up of 3 μl of PE-PanEV antibodies (1:66.7), 4 μl of Alexa Fluor® 488 anti-Pan Cytokeratin: C-11 (10 μg/ml; 1:50), 5 μl of Brilliant Violet 421™ anti-human CD45 Antibody: HI30 (1:40; all from Biolegend, Inc.), 5 μl of APC anti-PD-L1 antibody: MIH1 (1:40; Thermo Fisher Scientific, Inc.) and 5 μl of APC-Cy7 Mouse Anti-Human CD326 antibody: 9C4 (APC-Cy7 Mouse Anti-Human CD326 antibody; 1:40). To avoid a multiple plasma EV-EXÖBead® aggregation signal, individual beads from FSC-A and SSC-A were first gated. For the single positive EV subpopulation gating strategy, 'PanEV$^+$ and $CD45^{+ \text{ or } Neg}$', 'PanEV$^+$ and epithelial cell adhesion molecule $(EpCAM)^{+ \text{ or } Neg}$', 'PanEV$^+$ and $PD\text{-}L1^{+ \text{ or } Neg}$' or 'PanEV$^+$ and pan-cytokeratin $(PanCK)^{+ \text{ or } Neg}$' were further gated on Plasma EV-EXÖBead® complexes which based on the background signal from EF-EXÖBead® complexes. The final populations were expressed as a percentage of single beads. For the double positive EV subpopulation gating strategy, PanEV$^+$ and $CD45^{Neg}$ were gated on plasma EV-EXÖBead® complexes based on the background signal from EF-EXÖBead® complexes. PanEV$^+$ $CD45^{Neg}$ plasma EV-EXÖBead® complexes were further gated $EpCAM^{+/Neg}$ and $PD\text{-}L1^{+/Neg}$ also based on the background signal from EF-EXÖBead® complexes. The final four double positive populations of PanEV$^+$ $CD45^{Neg}$ EpCAM$^+$ $PD\text{-}L1^{Neg}$, PanEV$^+$ CD45N^{eg} EpCAM$^+$ PD-L1$^+$, PanEV$^+$ $CD45^{Neg}$ $EpCAM^{Neg}$ PD-L1$^+$ and PanEV$^+$ $CD45^{Neg}$ $EpCAM^{Neg}$ $PD\text{-}L1^{Neg}$ were expressed as percentages of single beads. For the triple positive EV subpopulation gating strategy, PanEV$^+$ and $CD45^{+/neg}$ were gated on Plasma EV-EXÖBead® complexes based on the background signal from EF-EXÖBead® complexes. Two populations of PanEV$^+$ $CD45^{Neg}$ and PanEV$^+$ CD45$^+$ EV-EXÖBead® complexes were further gated with $EpCAM^{+/Neg}$ and $PanCK^{+/Neg}$ also based on background signal from EF-EXÖBead® complexes. These four populations of PanEV$^+$ $CD45^{Neg}$ with $EpCAM^{+/Neg}$ and $PD\text{-}L1^{+/Neg}$ were further gated by PD-L1$^+$ population based on background signal from EF-EXÖBead® complexes. The final four triple positive populations of PanEV$^+$ $CD45^{Neg}$ EpCAM$^+$ $PanCK^{Neg}$ PD-L1$^+$, PanEV$^+$ $CD45^{Neg}$ EpCAM$^+$ PanCK$^+$ PD-L1$^+$, PanEV$^+$ $CD45^{Neg}$ $EpCAM^{Neg}$ PanCK$^+$ PD-L1$^+$ and PanEV$^+$ $CD45^{Neg}$ $EpCAM^{Neg}$ $PanCK^{Neg}$ PD-L1$^+$ were expressed as percentages of single beads. Another final four triple positive population of PanEV$^+$ CD45$^+$ EpCAM$^+$ $PanCK^{Neg}$ PD-L1$^+$, PanEV$^+$ CD45$^+$ EpCAM$^+$ PanCK$^+$ PD-L1$^+$, PanEV$^+$ CD45$^+$ $EpCAM^{Neg}$ PanCK$^+$ PD-L1$^+$ and PanEV$^+$ CD45$^+$ $EpCAM^{Neg}$ $PanCK^{Neg}$ PD-L1$^+$ also used the same gating strategy and were expressed as percentages of single beads. Significance was calculated by an unpaired t-test with Welch's correction. The specific test was selected based on number of groups, number of samples, and normality.

Intracellular EV marker and non-EVs marker staining. Non-EV fractions were collected after PPP incubation with EXÖBead®. To compare the non-EVs fraction to the plasma EV-EXÖBead® complexes, the non-EVs fraction were coupled to the same amount, number, and material of magnetic beads. The coupling steps consisted of first activating the magnetic particles with carboxyl groups (Chemicell GmbH) through incubation with 1-Ethyl-3-[3-dimethylaminopropyl] carbodiimide hydrochloride (EDC; Merck KGaA) in 0.1 M 2-(N-Morpholino) ethane sulfonic acid (MES; cat. no. M8250; Merck KGaA) at pH 5.0 for 30 min at 25˚C. Then non-EV fractions were covalent-coupled to the same number and same material of EDC activated carboxyl-group magnetic particles by incubation for 2 h at 25˚C. Non-EV-bead complex were further blocked by 0.5% EV-free BSA in PBS. A total of 1 ml of 10% EV-free BSA in PBS was coupled with EDC- activated carboxyl-group magnetic particles as a negative control. Plasma EV-EXÖBead® complexes, EF-EXÖBead® complexes, non-EV fractions-bead complexes and EF-bead complexes were then fixed by 200 μl of 4% paraformaldehyde in PBS for 10 min at 25˚C, penetrated by 200 μl of 0.1% Tween-20 in PBS for 10 min at 25˚C and blocked by 200 μl of 10% EV-free FBS in PBS (100,000 g, 4˚C for overnight centrifugation) for 30 min at 25˚C. Fixed/Penetrated plasma EV-EXÖBead® complexes, EF-EXÖBead® complexes, non-EV fractions-bead complexes and EF-bead complexes were further stained with 200 μl of 0.5% EV-free BSA in PBS with antibodies master mix at 25˚C for 1 h incubation. Antibodies master mix contained 2.5 μg/ml of Alexa Fluor® 488 anti-apolipoprotein A1/ApoA1 (1:40; clone: 2083A; R&D Systems, Inc.) and 5 μg/ml of PE anti-TSG101 (1:40; clone: EPR7130(B), Abcam). Antibodies-stained plasma EV-EXÖBead® complexes, EF-EXÖBead® complexes, non-EV fractions-bead complexes and EF-bead complexes were visualized by BD LSRFortessa™ (BD Biosciences) and data was analyzed with FlowJo V10.8 software (Tree Star, Inc.). The geometric mean fluorescence intensity (MFI) was used for the calculation. The initial MFIs of EF-EXÖBead® complexes and EF bead complexes were similar (data not shown). For the group of plasma EV-EXÖBead® complexes, the reduced MFI of the negative control was the MFI of the plasma EV-EXÖBead® complexes minus the MFI of the EF-EXÖBead® complexes. For the non-EV fraction bead complexes, the reduced MFI of

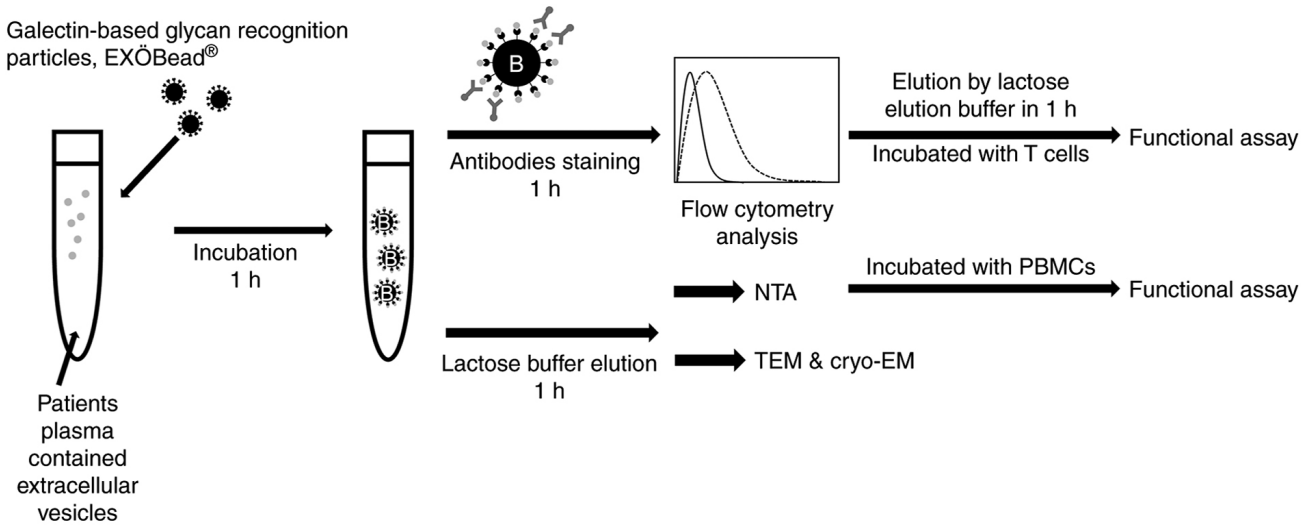

Figure 1. Workflow for extracellular vesicles isolation and analysis by using galectin-based glycan recognition particles, EXÖBead®.

the negative control was the MFI of the non-EV fraction bead complexes minus the EF bead complexes. Significance was calculated using an unpaired t-test.

Size-exclusion chromatography (SEC) was used qEV original 70 nm (IZON Science, Ltd.). EV fractions were collected from fraction 7 to 10 as recommends by the manual. A total of 500 μl of solution was collected per fraction. A total of 7 to 10 fractions were then pooled together as SEC-EVs (2 ml). To understand the total isolated components of SEC isolation, SEC was not concentrated by further steps such as ultracentrifugation or ultrafiltration. SEC EVs (2 ml) were coupled with the same amount, number and material of magnetic beads. SEC EVs were further coupled to 1-ethyl-3-(3-dimethylaminopropyl) carbodiimide (EDC) activated carboxyl group magnetic particles (Chemicell GmbH). A total of 1 ml of 10% EV-free BSA in PBS was also coupled with EDC-activated carboxyl group magnetic particles as a negative control. In the comparative study, plasma EV-EXÖBead® complexes, EF-EXÖBead® complexes, non-EV fraction bead complexes, and EF bead complexes were incubated with an antibody master mix in 200 μl of 0.5% EV-free BSA for 1 h at 25˚C. The antibody master mix contained 3 μl PE-PanEV (premixed CD9, CD63 and CD81 antibodies; 1:66) and 5 μl apolipoprotein A-I/ApoA1 Alexa Fluor® 488-conjugated antibodies (ApoA1; 1:40; cat. no. EP1368Y; Abcam). The initial MFIs of EF-EXÖBead® complexes and EF bead complexes were similar (data not shown). Plasma EV-EXÖBead® complexes, EF-EXÖBead® complexes, EF-bead complexes, and SEC-EV-bead complexes were visualized on BD LSRFortessa™ (BD Biosciences) and the data were analyzed using FlowJo software (Tree Star, Inc.). For the gating strategy, a gating population of beads was first determined based on FSC-A and SSC-A. Then, the PanEV$^{+/Neg}$ and ApoA1$^{+/Neg}$ populations were gated based on EF control. Significance was calculated using an unpaired t-test.

NTA. EV numbers and sizes were determined by ZetaView® Nanoparticle Tracking Analyzer PMX 110 (Particle Metrix GmbH). EVs were diluted in PBS to a final volume of 1 ml. For each measurement, two measurement cycles were performed by scanning 11 positions each and acquiring 60 frames per second under the following settings: pre-acquisition parameters were set to a sensitivity of 80; Shutter was set to 70. Cell temperature was set to 25˚C and trace length to 15 (20). After recording, the videos were analyzed with the built-in ZetaView software 8.05.11 SP1 (Particle Metrix GmbH) with specific analysis parameters: minimum particle brightness: 20; minimum size of 5 pixels, maximum size of 1,000 pixels and PSD nm/class of 10 and PSD classes/decade of 10.

TEM. A total of 5 μl of the undiluted sample were adsorbed for 60 sec to glow-discharged parlodion/carbon-coated copper grids. The grids were then blotted, washed 3 times with double-distilled water and negatively stained on two droplets of 2% uranyl acetate solution. Samples were imaged using a FEI Talos F200C TEM (FEI) operated at 120 kV. Electron micrographs were recorded on a Veleta Camera (EMSIS GmbH).

Cryo-TEM. A total of 4 μl aliquot of sample was adsorbed onto holey carbon-coated grid (Ted Pella, Inc.) blotted with Whatman 1 filter paper and vitrified into liquid ethane at -178˚C using a Leica GP plunger (Leica Microsystems GmbH). Frozen grids were transferred onto a Talos electron microscope (FEI) using a Gatan 626 cryo-holder. Electron micrographs were recorded at an accelerating voltage of 200 kV, using a low-dose system (20 e-/Å2) and keeping the sample at low temperature. Micrographs were recorded on a CETA camera (Thermo Fisher Scientific, Inc.).

Functional T cell assay. The functional assay was performed in CD4$^+$ immune cells of 3 patient blood sample in 3 replicates. CD4$^+$ cell extraction was performed from buffy coats obtained from the Blood Donation Center (Basel District) according to the manufacturer's protocol using the StraightFromTM Buffy Coat CD4 Micro Bead kit (product no; 130-114-980 MACS Miltenyi Biotec, Inc.). The T-cell activation was conducted according to the manual as described in the T Cell Activation/Expansion kit (product no. 130-091-441; MACS

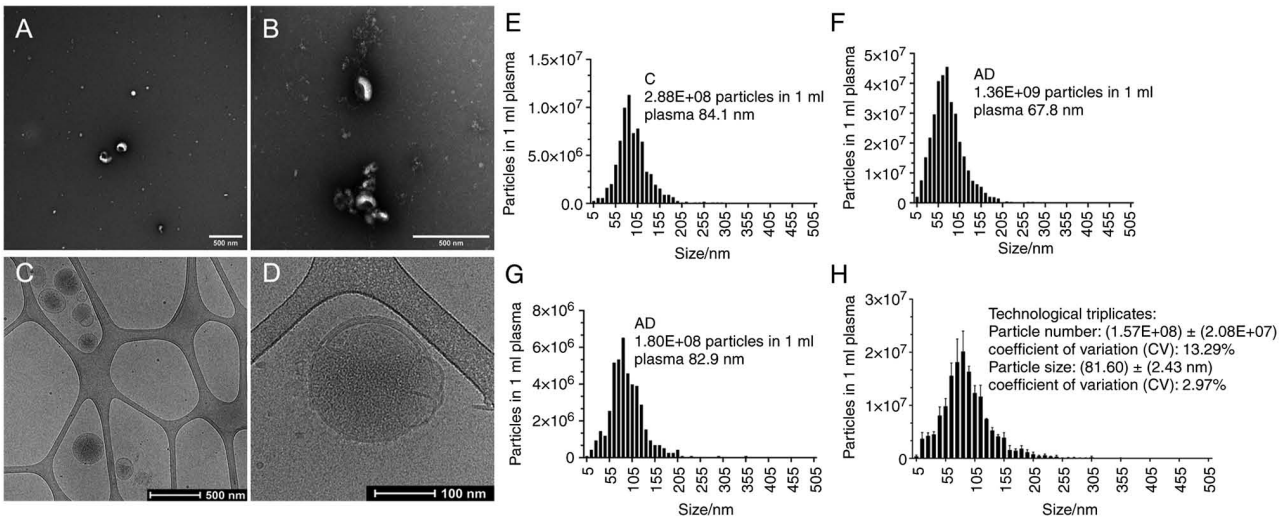

Figure 2. EV morphology and size distribution. (A and B) Eluted EVs by EXÖBead® isolation in transmission electron microscopy. (C and D) Eluted EVs by EXÖBead® isolation in cryo-electron microscopy. (E-G) Particle size distribution of eluted EVs by EXÖBead® isolation from three individual donors, measured with Zetaview®. (H) Particle size distribution of eluted EVs by EXÖBead® isolation from the same donor with three independent experiments, measured with Zetaview®. EV, extracellular vesicle.

Miltenyi Biotec, Inc.) (21,22). A total of 30 out of 200 μl eluted EVs isolated from tumor patient plasma were added to each well and gently mixed for 24 h at 37˚C. Cells were further stained with an antibody master mix containing 2.5 μl antibody/test of CD152 Monoclonal Antibody APC (Clone: 14D3), CD4 Monoclonal Antibody eFluor® 450 (Clone: SK3) and CD69 Monoclonal Antibody FITC: FN50 (all from Thermo Fisher Scientific, Inc.) for 50 min at 37˚C. Analytical assay was performed using flow cytometry (CytoFlex; Beckman Coulter, Inc.). Significance was calculated by non-parametric Kruskal-Wallis test with Dunn's multiple comparisons test.

Functional PBMCs assay. The functional assay was performed in PBMCs of different HNSCC patients' plasma EVs in technological triplicates. PBMCs were isolated from buffy coats received by healthy donors. PBMCs activation was conducted according to the manual as described in the T Cell Activation/Expansion kit (product no. 130-091-441; MACS Miltenyi Biotec, Inc.). Eluted EVs ($5x10^7$) isolated from tumor patient plasma were added to each well with $1x10^6$ PBMCs/ml in 1 ml culture medium and gently mixed for 24 h at 37˚C in the incubator. Lactose elution buffer (0.3 M lactose in PBS) was used as a negative control and as a gating base. To avoid the effect of the elution buffer, the total amount of CD69 was also examined in the elution buffer treatment group and in the group with only activated T cells. The total CD69 amount did not differ between elution buffer with T-cell activation stimulation and T-cell activation stimulation only (data not shown). Cells were first stained at 100 μl at a 1:100 ratio with the cell viability dye Zombie NIR™ for 30 min at 25˚C (Biolegend, Inc.). After two washing steps, cells were stained with 100 μl of 1:100 antibody master mix, CD4 Monoclonal Antibody eFluor® 450 (Clone: SK3, Thermo Fisher Scientific, Inc.), APC anti-PD-L1 antibody: MIH1 (Thermo Fisher Scientific, Inc.), PE anti-human CD279 (PD-1) Antibody: EH12.2H7 (Biolegend Inc.) and CD69 Monoclonal Antibody FITC: FN50 (Thermo Fisher Scientific, Inc.) for 30 min at 4˚C. Analytical assay was performed using flow cytometry: BD LSRFortessa™ (BD Biosciences) and flow data were analyzed by FlowJo software (Tree Star, Inc.). First, the lymphocyte population was recorded based on FSC-A and SSC-A. Then, the population of individual cells was detected based on FSC-A and FSC-H. To identify live cells, the zombie NIR negative population was gated. To examine live T cells, the $CD4^+$ population was then gated. The final gate was gated to $CD69^{+/Neg}$ with $PD1^{+/Neg}$ or $CD69^{+/Neg}$ with $PD\text{-}L1^{+/Neg}$. Significance was calculated by Brown-Forsythe and Welch's ANOVA test with Dunnett's T3 multiple comparisons test.

Statistical analysis. Flow cytometry data including gating were performed by FlowJo version 10.8 software (Tree Star, Inc.). Data were statistically analyzed with Prism version 8 (GraphPad Software, Inc.). The specific test used is described in the figure legend. $P<0.05$ was considered to indicate a statistically significant difference.

Results

Morphology and particle number of eluted EVs by magnetic galectin-based glycan recognition particles (EXÖBead®) isolation. To compare whether the eluted EVs were similar in size to those reported in the literature (23) the morphology was examined after isolation of EXÖBead® and elution in lactose-PBS buffer in conventional TEM, where they were observed as intact, cup-shaped, membrane-bound vesicles with a size of 30-200 nm (Fig. 2A and B). Eluted EVs were observed as a double lipid layer of vesicles in cryo-EM with a size of 30 nm-250 nm (Fig. 2C and D). ZetaView (Particle Metrix, Inning am), a NTA instrument, was used to measure the yield and size of nanoparticles from three individual donors as biological triplicates (Fig. 2E-G) and three technological triplicates of a same donor (Fig. 2H). The medium size of eluted EVs from three technological triplicates was 81.6±2.43 nm (CV: 2.97%; Fig. 2E-G). The total particle number from 1 ml

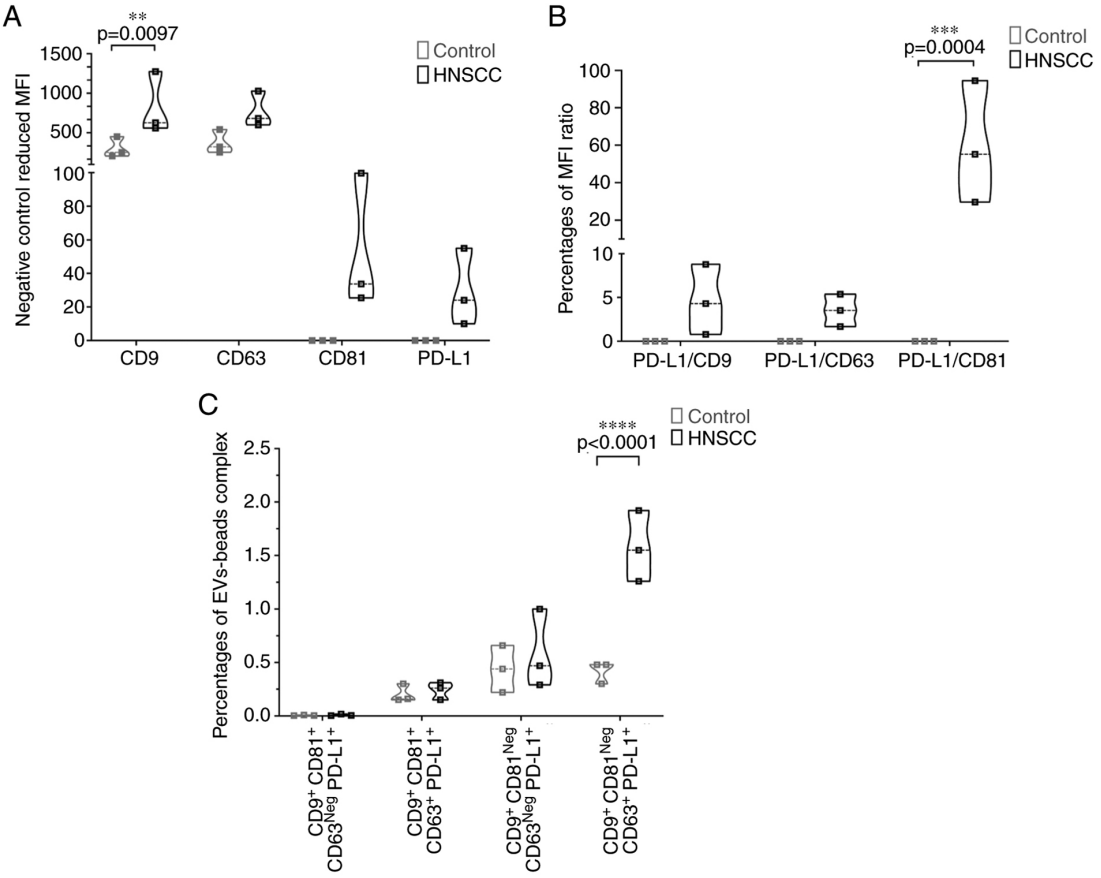

Figure 3. Bead-based flow cytometric analysis of EV surface markers. (A) EV surface markers of plasma EV- EXÖBead® complexes (patients: n=3 and healthy controls: n=3) are shown as reduced geometric MFI of CD9, CD63, CD81 and PD-L1 in the negative control. (B) Plot of the ratio of the MFI of PD-L1 to the MFI of CD9, the MFI of PD-L1 to the MFI of CD63, and the MFI of PD-L1 to the MFI of CD81. (C) $CD9^+$ $CD81^+$ $CD63^{Neg}$ $PD\text{-}L1^+$, $CD9^+$ $CD81^+$ $CD63^+$ $PD\text{-}L1^+$, $CD9^+$ $CD81^{Neg}$ $CD63^{Neg}$ $PD\text{-}L1^+$ and $PD\text{-}L1^+$ $CD9^+$ $CD81^{Neg}$ $CD63^+$ of plasma EV-EXÖBead® complex were gated with FlowJo™. Significance was calculated by Two-way ANOVA with Šídák's multiple comparisons test. EV, extracellular vesicle; MFI, mean fluorescence intensity.

plasma of 3 technological triplicates was $1.57x10^8 \pm 2.8x10^7$ (CV: 13.29%; Fig. 2H). The eluted EVs from EXÖBead® isolation represented reproducible and high similarity as mentioned in the literature (23).

EV surface marker, intracellular marker and non-EV marker. The recovered EVs were analyzed and checked for established EV surface markers by bead-based flow cytometry. $CD63^+$, $CD9^+$ and $CD81^+$ were reported as common and MISEV compliant EV surface markers (23). Geometric MFI of CD63, CD9 and CD81 was expressed on recovered EXÖBead® isolates and was increased in HNSCC patients compared with healthy donors for all surface markers (Figs. 3A and S1). MFI of $CD9^+$ was significantly higher in patients with HNSCC compared with the healthy controls (P=0.0097; Figs. 3A and S1A). In addition, MFI of $PD\text{-}L1^+$, an important diagnostic cancer and surface marker (24) was increased in HNSCC tumor patients compared with the healthy controls. Relative ratio of $PD\text{-}L1^+$ MFI versus $CD81^+$ MFI (P=0.0004) was significantly higher in patients with HNSCC compared with the healthy controls (Fig. 3B) in both cases. $PD\text{-}L1^+$ $CD9^+$ $CD63^+$ $CD81^{Neg}$ EVs-EXÖBead® complex from HNSCC patients had also higher relative scores (P<0.0001; Figs. 3C and S1B-E). However, $PD\text{-}L1^+$ $CD9^+$ $CD63^+$ $CD81^+$, $PD\text{-}L1^+$ $CD9^+$ $CD63^{Neg}$ $CD81^+$ and $PD\text{-}L1^+$ $CD9^+$ $CD63^{Neg}$ $CD81^{Neg}$ EVs-EXÖBead® complex showed no difference between the two groups (Figs. 3C and S1B-E). These population changes suggested that $PD\text{-}L1^+$ $CD9^+$ $CD63^+$ EVs may play an important role in HNSCC, but further research is required to support or refute this assumption. In addition to extracellular markers, TSG101 was additionally measured as typical intracellular EV marker (23). The experiments were well feasible and TSG101 could be detected in EVs of HNSCC after isolation and recovery by EXÖBead®. The levels of the isolates were significantly increased in the EXÖBead® fraction compared with the unbound patient plasma (P=0.015; Figs. 4A and S2A). A frequent problem of EV isolation is the contamination by protein aggregates or other aggregates/particles from blood samples, due to the complexity of blood composition (23). A well-established marker for contamination in EV preparations is ApoA1 (23). The ApoA1 concentration was high in residual plasma with MFI 7000 compared with almost none in the EXÖBead® fraction (P=0.0002; Figs. 4A and S2A). To gain an improved understanding of the specificity of EV isolation, SEC was compared with EXÖBead® in terms of PanEV and ApoA1 protein presence. $PanEV^+$ $ApoA1^{neg}$ population was significantly higher in the EV-EXÖBead® complex compared with the EV-SEC beads complex (P=0.019; Figs. 4B and S2B). While $PanEV^{neg}$ $ApoA1^+$ population was significantly higher in EV-SEC beads complex compared with EV-EXÖBead®

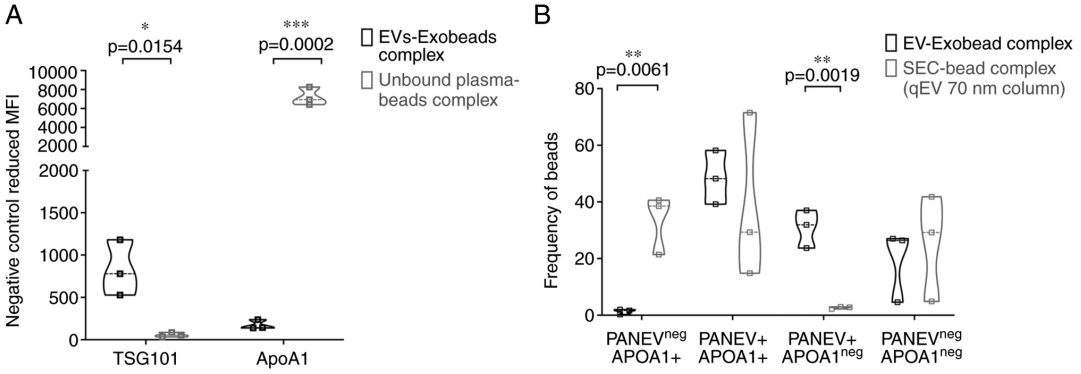

Figure 4. Bead-based flow cytometry analysis of EV intracellular marker and non-EV marker. (A) Intracellular EVs markers (TSG101) and non-EV markers (ApoA1) of plasma EVs-EXÖBead® complexes and unbound plasma fraction magnetic bead complexes (n=3) are shown as reduced geometric mean fluorescence intensity in the negative control. (B) PanEV$^{+/Neg}$ and ApoA1$^{+/Neg}$ populations of the plasma EVs-EXÖBead® complex and SEC (Izon qEVoriginal 70) plasma EVs-magnetic beads complex are expressed as percentages by gating with FlowJo™. Significance was calculated using an unpaired t-test. EV, extracellular vesicle.

complex (P=0.0061; Figs. 4B and S2B). This flow cytometric result of EV-EXÖBead® complex suggested that measurable lipoprotein contamination may be lower with EXÖBead® isolation of plasma EVs than with isolation by SEC method. Notably, PanEV^{+} ApoA1^{+} population may be detected by both isolation methods with no significant difference (23,25).

HNSCC specific exosomal markers. A specific set of serum markers for diagnosis and therapeutic purpose in HNSCC patients is currently lacking (26). CD45, EpCAM, PanCK and PD-L1 have been reported as potential biomarkers in HNSCC patients and their isolated EVs/exosomes (11,24). However, the expression level of CD45, EpCAM, PanCK and PD-L1 on EVs in HNSCC patients remains unknown. EXÖBead® was used to isolate EVs from plasma which were then stained with the master mix of antibodies containing PanEV, CD45, EpCAM, PanCK and PD-L1. The expression level of EpCAM^{+} in HNSCC patients was significantly higher than in healthy controls (P=0.023) while there was no significant difference in the other markers when considered independently (Figs. 5A and S3A). To accurately determine the percentage of tumor-specific EVs in the circulation, single EV bead complexes were next gated to exclude multiple EV bead complexes and examine the difference between HNSCC patients and healthy controls. In the antibody staining of the obtained EVs, the results of EV-EXÖBead® complex showed that there was a significant difference between CD45^{neg} PanEV^{+}, EpCam^{+} PanEV^{+} and PDL1^{+} PanEV^{+} between patients with HNSCC and healthy controls (CD45^{neg} PanEV^{+}, P=0.026; EpCAM^{+} PanEV^{+}, P=0.004; PD-L1^{+} PanEV^{+}, P=0.007) (Figs. 5B-D and S3B-D). The EV-EXÖBead® complex stained with PanCK showed no significant difference between HNSCC and control (Figs. 5E and S3E). The EV-EXÖBead® complex population of CD45^{neg} EVs that was EpCAM^{+} and PD-L1^{+} was significantly increased in HNSCC patients compared with the control group (P=0.002; Fig. 5F and Fig. S3F-I). The same was found for the group of EV-EXÖBead® complex which was CD45^{neg}, EpCAM^{+} and PD-L1^{neg} (P=0.003; Figs. 5F and S4F-I). For this purpose, CD45^{neg}, EpCAM$^{+/neg}$, PD-L1$^{+/neg}$ and PanEV^{+} were gated on a single EV beads complex (Fig. 5F and S3F-I). In addition, the triple positive population on the EV-EXÖBead® complex was examined. It was found that CD45^{neg} EV-EXÖBead® complexes that were double or triple positive for the markers EpCAM, PD-L1 and PanCK were significantly more expressed in HNSCC than in healthy controls [(EpCAM^{+}, PD-L1^{+} and PanCK^{neg}; P=0.0005) (EpCAM^{+}, PD-L1^{+} and PanCK^{+}; P=0.02; Figs. 5G and S3J-M)]. Notably, it was also identified that CD45^{+} EV-EXÖBead® complexes with EpCAM^{+}, PD-L1^{+}, but PanCK^{-} were detectable to a significantly higher extent in HNSCCs than in healthy controls (P=0.025; Figs. 5H and S3N-Q). These significantly altered populations of EV-EXÖBead® complex suggested that single positive EVs, double positive EVs or triple positive EVs may play an important role in the progression of HNSCC. Further studies need to be performed. To demonstrate yet again that EVs were specifically isolated with the method described in the present study, particle size and number of particles were checked in parallel with the analysis of specific markers on the EVs with NTA. Similar particle sizes were found in both groups (HNSCC: 125.2±9.1 nm; control: 123.32±7.42 nm). The particle number was comparable (HNSCC: $2.54x10^{8}$±$1.27x10^{8}$; control group: $5.58x10^{8}$±$3.17x10^{8}$) (Fig. 5I).

Functional in vitro competence of plasma-derived EVs. To evaluate the biological activity and functional *in vitro* competence of EVs isolated and recovered from plasma of tumor patients, EVs obtained by EXÖBead® as well as EVs obtained by polyethylene glycol (PEG)-based precipitation method was co-incubated with activated T cells (CD4^{+} T cells) and compared with activated T cells without EV co-incubation. The aim was to measure the *in vitro* immunosuppressive capacity of EVs isolated by the established PEG-based precipitation method (27,28) and compare it to the immunosuppressive capacity of EVs isolated by EXÖBead®. In the present study, the purity of CD4^{+} T cells was at least 90%, analogous to analyses in older proprietary trials (6). Percentage of CTLA4^{+} CD69^{neg} T responder cells was measured by flow cytometry (29,30) after co-incubation with EVs isolated by the two different methods. A highly significant difference was observed between untreated activated T cells and T cells treated with 30 out of 200 μl

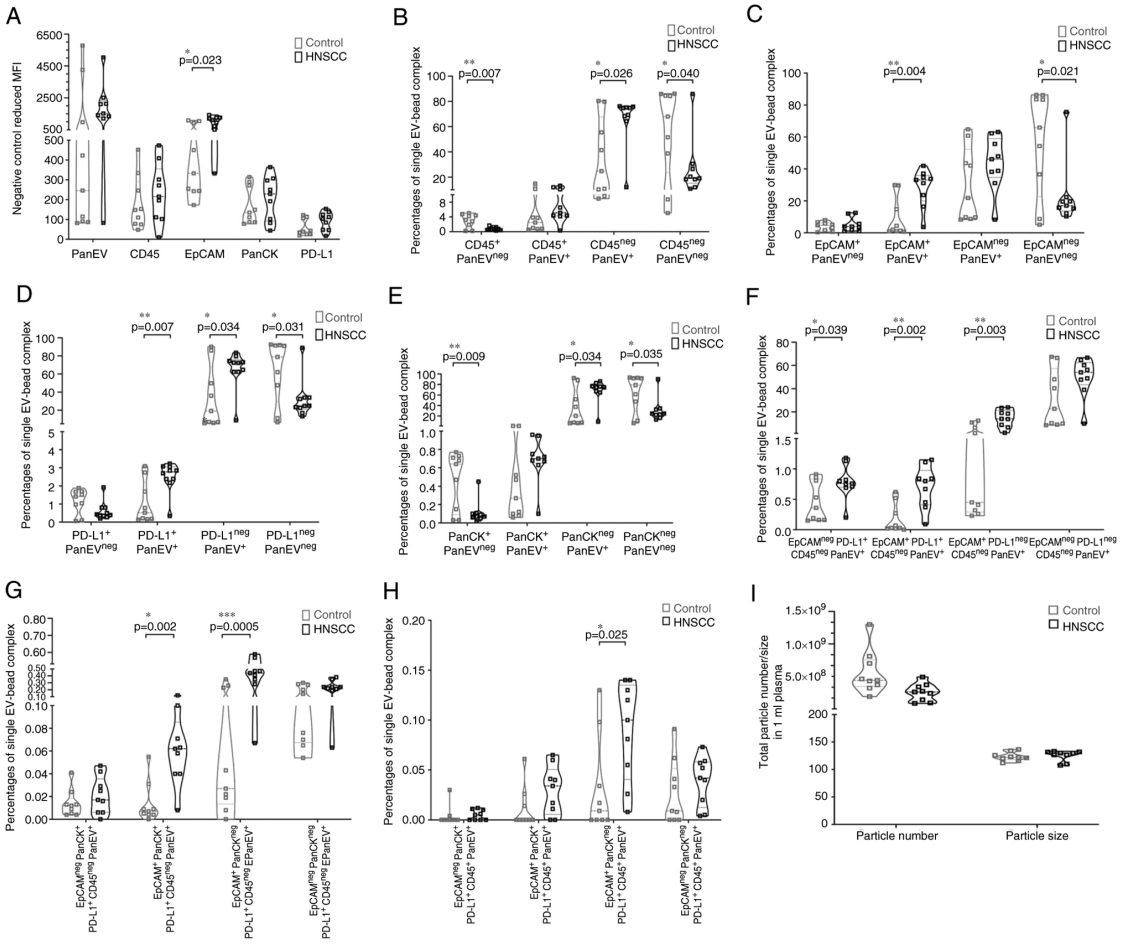

Figure 5. Bead-based flow cytometric analysis of HNSCC biomarkers. (A) EVs surface marker (PanEV), leukocyte common marker (CD45) and HNSCC markers (EpCAM, PanCK and PD-L1) of plasma EVs-EXÖBead® complexes (patients: n=9 and healthy controls: n=9 are shown as reduced geometric mean fluorescence intensity in the negative control. (B) PanEV$^{+/Neg}$ CD45$^{+/Neg}$. (C) PanEV$^{+/Neg}$ EpCAM$^{+/Neg}$. (D) PanEV$^{+/Neg}$ PD-L1$^{+/Neg}$. (E) PanEV$^{+/Neg}$ PanCK$^{+/Neg}$. (F) CD45^{neg} PanEV^{+} EpCAM$^{+/Neg}$ and PD-L1$^{+/Neg}$. (G) CD45^{neg} PanEV^{+} PD-L1^{+} EpCAM$^{+/Neg}$ and PanCK$^{+/Neg}$. (H) CD45^{+} PanEV^{+} PD-L1^{+} EpCAM$^{+/Neg}$ and PanCK$^{+/Neg}$ of single plasma EVs-EXÖBead® complex were evaluated using FlowJo™. Significance was calculated using an unpaired t-test with Welch's correction. (I) Particle number and size from HNSCC (n=9) and control plasma (n=9) are measured by Zetaview®. Significance was calculated using Kolmogorov Smirnov test. EV, extracellular vesicle; HNSCC, head and neck squamous cell carcinoma; PanCK, pan-cytokeratin; EpCAM, epithelial cell adhesion molecule.

EXÖBead®-isolated EVs in terms of CTLA4 and CD69 expression (P=0.025; Fig. 6A and S4A). Notably, this effect was not observed when activated T cells were treated with EVs obtained by PEG-based isolation (Figs. 6A and S4A). There was no difference of single CTLA4^{+} CD4^{+} T cells within these three groups (Fig. S4B). To address the question of whether EVs isolated from plasma of patients with HNSCC using EXÖBead® retain their biological activity, EVs from different patients were examined for immunosuppression. The present data showed that PD-L1^{+} CD69^{neg} CD4^{+} T cells were significantly increased after co-incubation with 5x10^{7} plasma EVs from HNSCC patients (n=13, with technological triplicate) compared with co-incubation with elution buffer (technological triplicate) (P=0.0011) and healthy donors (n=3, with technological triplicate) (P=0.0045) as controls (Figs. 6B and S4C). It was also found that PD-L1^{+} CD69^{neg} CD4^{+} T cells were also higher in treatment with healthy controls' EVs compared with controls (P=0.0404; Figs. 6B and S4C). Notably, it was also found that PD1^{+} CD69^{neg} CD4^{+} T cells were also significantly increased in patients' group compared with the elution buffer group (P=0.0344), but there was no difference between healthy controls and elution buffer group (Fig. S4D). No difference was observed between the groups of patients and controls and elution buffer from signal positive of CD69, PD1 and PDL1 CD4^{+} T cells (Fig. S4E). Thus, by isolating EVs with EXÖBead® it appeared to be possible to isolate functionally competent EVs from plasma of HNSCC patients.

Discussion

Over the past decade, interest in EVs as biomarkers for tumor disease has markedly increased. This is also true for malignancies of the head and neck, particularly the most common entity of HNSCC. Unfortunately, numerous patients with HNSCC are already at an advanced stage at the time of diagnosis, so a tool for earlier initial diagnosis, as well as for recurrence detection and therapy monitoring, would be of great clinical value. There is still a long way to go before EVs are regularly used clinically as tumor markers, although much has already been learnt about their biomarker potential (31).

One of the problems being faced in integrating into clinical practice is the development of a simple, rapid, and reproducible method to reliably isolate pure EVs from patient plasma.

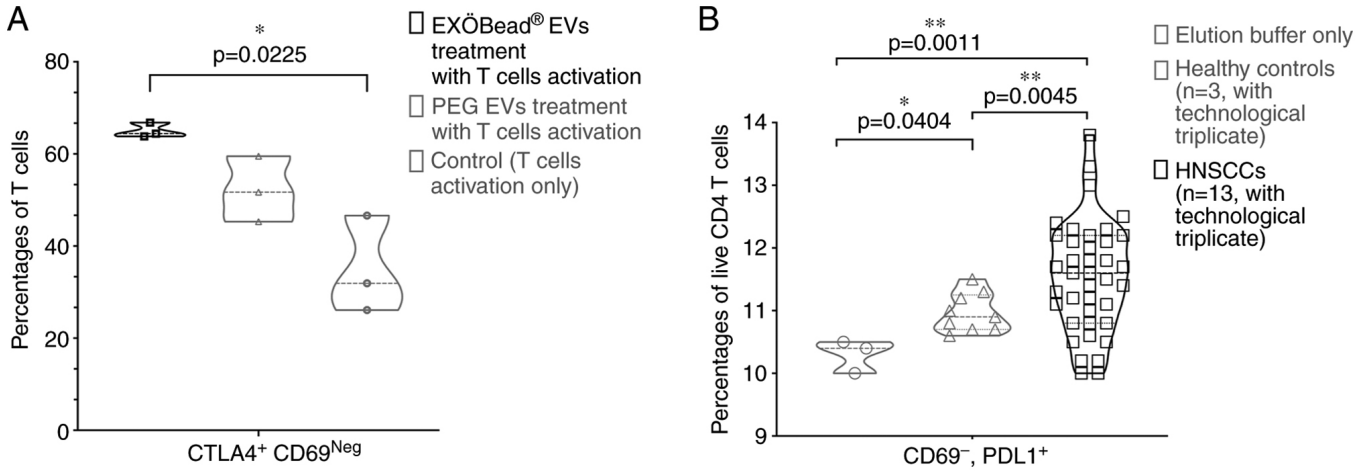

Figure 6. EVs functional assay of T cells and PBMCs activation. (A) A total of 30 out of 200 μl eluted patient plasma EVs from EXÖBead® isolation and PEG EVs were treated with CD4+ T cells in anti-CD2/3/28 antibodies activation condition. The Violin plot shows that CTLA4+ CD69Neg T cells emerged only when treated with eluted patient plasma EVs from EXÖBead®, PEG EVs and T cells activation. Significance was calculated by non-parametric Kruskal-Wallis test with Dunn's multiple comparison test. (B) a total of $5x10^7$ particles of eluted patient or control plasma EVs from EXÖBead® isolation were treated with $1x10^6$ PBMCs (ratio: 50:1) under anti-CD2/3/28 antibody activation conditions. Violin plot showed that CD69+ PD-L1+ live CD4+ T cells were derived from treatment with elution buffer alone, from plasma EVs from HNSCC patients (n=13, with technological triplicate) and from EVs from healthy controls (n=3, with technological triplicate). Significance was calculated by Brown-Forsythe and Welch's ANOVA test with Dunnett's T3 multiple comparisons test. EV, extracellular vesicle; PBMC, peripheral blood mononuclear cells.

In the present study, a novel galectin-coupled magnetic bead method was used to isolate pure EVs from human plasma. Intact eluted EVs were examined in detail by TEM imaging and cryo-EM, and the characteristic EV shell shape was confirmed. Size and concentration measurements by NTA showed low variability and high reproducibility in all process triplets. In accordance with MISEV 2018 guidelines, extracellular and -intracellular EV protein markers and non-EV markers were fully validated by flow cytometry (23).

Our result firstly showed that galectin-coupled magnetic beads (EXÖBead®) isolated EVs from plasma with low contamination of lipoprotein. In a second step, lactose-based elution buffer was used to successfully obtain functionally intact EVs after elution. Galectins are glycan-binding proteins and contain C-terminal carbohydrate recognition domains that preferentially bind β-galactoside-rich glycoprotein (32).

Polylactosamine, α2,6-linked sialic acid, high mannose N-glycan, and complex-type N-glycan were previously shown to be present on the surface of EVs in enriched form (33,34). Previous studies showed that EVs from ovarian cancer cells accumulate galectin-3-binding protein (LGALS3BP), which contains a large amount of sialylated complex-type N-glycans (17,19). In our view, this highlights the potential application of an isolation method for EVs based on galectin-based glycan recognition.

Research conducted both in-house and by other research group indicated that protein levels of EVs isolated from plasma of HNSCC patients were significantly higher than those from healthy donors (10,11). Ludwig *et al* (9) also showed that the increase in total plasma EVs correlated well with disease activity. However, in numerous of these studies, SEC was used as a purification method to isolate EVs from patient plasma. Meanwhile, it is known that SEC is not only used to isolate EVs, but also to purify high amounts of lipoprotein (25). This fact may prove somewhat problematic in the future, as Chen *et al* (35) demonstrated that only exosomal biomarkers show a correlation with disease progression. Therefore, the specificity of EV isolation is of particular importance in this context. Using an isolation method for EVs based on galectin-based glycan recognition (EXÖBead®), measurable lipoprotein contamination was markedly lower when isolating exosomes from plasma than when isolating them using the SEC method. This was reflected in the higher concentration of PanEV+ ApoA1neg population in the EXÖBead® isolation fraction compared with the SEC isolation fraction while it was the opposite in PanEVneg ApoA1+ population. It was also observed that particle numbers from SEC isolation were 100-200 times higher than EXÖBead® isolation from our unpublished results. When the particle number and bead-based flow cytometric data were combined, it was considered that SEC isolates a larger amount of lipoprotein compared with EXÖBead®. Fluorescent NTA and antibody-stained EV flow cytometry was used to determine which particles are pure EVs and which particles are lipoproteins in SEC and EXÖBead®. Notably, the PanEV+ ApoA1+ population could be detected by both isolation methods without significant difference. PanEV+ ApoA1+ may indicate that small EVs carry ApoA1 protein or that high-density lipoprotein carries PanEV proteins. It has already been revealed that EVs isolated from plasma can be covered with low-density lipoprotein (36-38). In addition, lipoproteins such as ApoA, ApoB and ApoE could be detected on EVs of pigment cells (39), making it difficult to distinguish between lipoprotein particle contaminants and EV-associated lipoproteins (25). Thus, a precise classification of the function of the PanEV+ ApoA1+ population is not yet possible. To demonstrate PanEV+ ApoA1+ population, further preparation of 'pure EVs isolation from cell cultures' and 'pure EVs isolation from lipoprotein overexpression cell cultures' will be required in future studies. Another limitation is that most of EVs studies did not measure lipoprotein level before EV isolation. The lipoprotein

level should be also considered before EV isolation in the future. Therefore, particularly in this still early phase, purity in the workup is considered to be particularly important for diagnostic and prognostic statements. Our research to date has shown that lipoprotein levels can be significantly reduced by isolation based on galectin-based glycan recognition compared with unbound plasma.

An interesting and important observation in the present study was that a T-cell activation assay could show that EVs maintained their functional activity throughout the isolation process with EXÖBead®. Eluted EVs from patients showed a stronger suppressive character after isolation based on galectin-based glycan recognition than with the conventional isolation method using PEG. Since our EVs were obtained from the same patients at the same time point, it was postulated that they lose a greater proportion of their functional activity during conventional isolation. This difference may play an important role in functional assays of EVs. While the concentration and expression patterns of tumor-derived EVs already provide us with important information, functional assays play an important role in understanding how tumors interact with the immune system.

It is now known that EVs can tell us a lot about their mother cells by their expression pattern (11). However, the interaction between tumor and immune system is markedly more complex to be characterized by surface patterns alone. Our understanding can become more improved, as closer it gets to the '*in vivo* activity' of EVs. Thus, isolated EVs should retain their biological activity as much as possible. It is considered that the galectin-based glycan recognition method provides a good basis for this, although further and broader studies will be needed. For example, it was identified that CTLA4^{+} CD69^{neg} increases to a greater extent in activated T cells in co-incubation experiments with EXÖBead® than in co-incubation experiments with a conventional assay (PEG isolation). Since only 30 out of 200 μl eluted EVs were used, fixed particles number/T cells for CTLA4$^{+/Neg}$ CD69$^{+/neg}$ T cells experiment will also be examined in the future. The results showed that PD-L1^{+} CD69^{+} T cells were significantly higher in treatment with patient's plasma EVs (EV versus PBMCs ratio: 50:1) compared with healthy controls and elution buffer only. Theodoraki *et al* (24) showed that PD-L1^{+} exosomes were highly correlated with disease progression (24). CD69^{+} CD8^{+} T cells were significantly lower when treatment with PD-L1^{+} high exosomes compared with PD-L1^{+} low exosomes (24).

The present data showed the similar suppression effect on increasing of PD-L1^{+} CD4^{+} T cells in treating with patients' plasma EVs compared with controls. However, no changes of CD69^{+} CD4^{+} T cells were observed between treatment with patients' EVs, controls' EVs and elution buffer only. One possibility may be that HNSCC patients were not separated into different stages. Further studies will need to demonstrate if CD69^{+} CD4^{+} T cells are reduced by treatment with later stages of patients' plasma EVs. Knowing that CTLA4 and PD1/PD-L1 is a suppressive marker and CD69 is an activating marker, it can be assumed that EVs isolated with EXÖBead® have a suppressive character and thus probably an improved-preserved functionality. This allows reliable co-incubation experiments with EVs from tumor patients and immune cells, which is considered necessary to elucidate tumor-immune interaction via EVs in an improved way. Understanding which types of regulatory T cells were induced by patient's plasma EVs will also be an interesting research subject. Further study will be needed to identify by different regulatory T cells markers, such as CD25 and Foxp3 (40).

In patients with tumor disease, 2 major producers of EVs have been previously identified. One is the metabolically active tumor cells themselves and the other is the immune cells (41-43). To classify these different groups of EVs based on their surface markers, plasma EVs were first divided into two main subgroups. First, those that are mainly tumor-associated released (CD45^{neg}) and second, EVs released by immune cells (CD45^{+}). Immunologically hot tumors-i.e., those with a high number of tumor-infiltrating lymphocytes (TILs)-tend to have an improved response to primarily immunotherapies (44,45). To infer from this that there are good immune cell-derived EVs and bad tumor cell-derived EVs would fall far short. Not least because immune cell derived EVs-like immune cells themselves-appear to play a dual role in tumorigenesis and progression (46). Several studies on TILs suggested that they play an important role in HNSCC progression (47,48). As early as 2007, Rajjoub *et al* (49) published studies on the prognostic significance of CD3low TILs in oropharyngeal cancer. An association between this subset of T cells and a high rate of metastasis was revealed. By contrast, Badoual *et al* (50) showed that the enrichment of tumor-infiltrating CD4^{+}CD69^{+} T cells correlates with improved survival. Thus, how exactly TILs contribute to HNSCC progression is not yet well understood and it is considered that isolation and analysis of EVs coming from TILs may contribute to an improved understanding of HNSCC progression. According to our literature search, studies regarding the role of TIL-derived EVs and their role in HNSCC are still very sparse. In the present study, the group of CD45^{+} EVs that were simultaneously positive for EpCAM and PD-L1 was significantly increased in the HNSCC group compared with healthy controls. Although further and more in-depth studies are needed, this triple staining may contribute to an improved understanding and, in perspective, may be an option for monitoring disease progression.

In the bead-based flow cytometric analysis of EVs isolated from human plasma using galectin-based glycan recognition as isolation method, 3 common EV surface markers (CD9, CD63, and CD81), an intracellular EV marker (TSG101) and 3 HNSCC biomarkers (PD-L1, PanCK, and EpCAM) were searched for. The bead-based flow cytometry result showed PD-L1^{+} CD9^{+} CD63^{+} CD81^{Neg} EVs-EXÖBead® complex was significantly higher in HNSCC patients compared with healthy controls. However, it was only tested in small samples size and these antibodies pair shall be examined with a large samples size in the future. The bead-based flow cytometry suggested that ApoA1 were low in the EV-EXÖBead® complex, whereas these were detectable to a markedly higher extent in the unbound plasma. In the present choice of biomarkers for HNSCC, it was not possible to rely on any established serum biomarker to date, such as exists with prostate specific antigen in prostate cancer or thyroglobulin in thyroid cancer. Nevertheless, there are a number of molecules in HNSCC that have received increasing attention in previous years and may have prognostic value (51-53). These considerations formed the basis for the choice of the markers selected and their combination. The

bead-based flow cytometry suggested 5 biomarker panels to be the future of EV-based liquid biopsy and some potential was observed in the selected markers based on the present data. Beads-based flow cytometry and sub-population gating strategy can help to easily/fast understand the expression profiles of each marker and sub-populations of EVs. However, antibodies-stained EV-EXÖBead® complex was analyzed instead of EVs directly. Further researches will be needed in the future, such as EV flow cytometry next-generation sequencing and proteomics.

For numerous years, PD-1 or PD-L1 has received marked attention in cancer research (54). For HNSCC, for example, it has been identified that there is an association between PD-1 and PD-L1 overexpression and tumor progression (55). For numerous years, target therapy with checkpoint inhibitors in HNSCC was mainly experimental in nature. PD-1/PD-L1 inhibitors were taken out of this niche by the Keynote-048 study, which showed that the checkpoint inhibitor pembrolizumab is superior to the previously established EXTREME study (cetuximab, cisplatin, 5 FU) in metastatic and/or relapsed HNSCC in combination or as monotherapy (56,57). However, since not all patients respond equally to this approach, PD-L1 status is used to subtype patient groups. For this purpose, immunohistochemical examinations are performed on tissue samples and scores are generated to predict response to immunotherapy. Although there is a certain correlation, the predictive character of these examinations still needs improvement. Since the tumor is constantly changing during the course of the disease and particularly under the selection pressure of tumor therapy, good therapy monitoring requires regular analysis of the tumor expression pattern. However, frequent biopsies are associated with increased morbidity for patients. Regular characterization of the tumor should therefore be performed by blood sampling. In our opinion, exosomal PD-L1 is suitable for this purpose and can be determined quickly and reliably using the EXÖBead® isolation technique.

Notably, pretreatment high exoPD-L1 levels but not soluble PD-L1 levels were shown to be associated with disease progression (24) in patients with HNSCC. A similar observation was made by Chen *et al* (35) in studies of patients with metastatic melanoma. When examining the levels of different types of PD-L1 (total soluble, micro vesicular, exosomal, and secreted or excreted PD-L1) before and after immunotherapy, the levels of exoPD-L1, but not other forms of PD-L1, differed between patients who would respond to PD1 blockade. Early after initiation of immunotherapy, the magnitude of the increase in exoPD-L1 was significantly higher in responders, whereas a non-significant difference was observed for the other types of PDL1 (35). Whether this increase in exoPD-L1 was due to the release of exosomes from tumor cells or immune cells, or even both, requires further investigation of plasma EVs. These findings, together with a simplified and reliable isolation technique, may allow a more precise selection of patients who will benefit from immunotherapy in the future.

However, other molecules also have the potency of prognostic relevance. EpCAM is a known tumor-associated antigen that is highly overexpressed on various squamous cell carcinomas including HNSCC (48). The expression level of EpCAM on isolated EVs was significantly higher in HNSCC patients than in healthy controls, whereas there was no significant difference in the other markers when considered independently. The present findings confirmed data published by Theodoraki *et al* (58), which showed significantly higher EpCAM expression on $CD45^{neg}$-EVs by separation of CD45 antibody beads base isolation. Analyses of the MFI of EpCAM, a number of complexes also showed a significantly higher percentage in patients with HNSCC than in healthy patients.

In our studies, it was observed that the quadruplex of EVs that were $CD45^{neg}$, $PanEV^{+}$, $EpCAM^{+}$, $PanCK^{+}$, and $PD\text{-}L1^{+}$ was significantly higher in HNSCC patients compared with EVs from healthy controls. This fact allowed to hypothesize that this may be the population of tumor-derived EVs and thus the combination of different markers may allow higher accuracy in subdividing different subsets of EVs. Notably, it was also found that $CD45^{+}$ EVs, which were $EpCAM^{+}$, $PD\text{-}L1^{+}$ but $PanCK^{neg}$ were significantly more detectable in HNSCCs than in healthy controls. This may indicate that these are EVs from tumor-infiltrating lymphocytes.

While some prognostic potential was observed for individual markers (PD-L1 and EpCAM) when considered separately, it is the combination of the various markers with the gating strategy used that appears to allow more accurate differentiation between the various EV subpopulations.

Further studies with larger numbers of patients will be needed to examine this hypothesis in more depth, but it is hypothesized that in such a validation cohort the combination of markers may increase the prognostic potential in HNSCC. Because the membrane-bound proteins are also a reflection of the cancer and can be obtained from a simple blood sample, they also provide a source for functional studies to understand in an improved way the biological mechanisms of exosomal membrane-bound proteins in HNSCC and cancer in general.

Using a galectin-based glycan recognition (EXÖBead®) as isolation method with a 5-antibody staining panel, it was possible to identify tumor-specific EV populations. A distinction between infection/inflammation and tumor is also conceivable, although this requires considerably more investigation. However, if this assumption is confirmed it could be of great help in clinical practice particularly in the differentiation of post-therapeutic inflammation and tumor recurrence. There are also certain limitations. At the moment, EXÖBead® is only available for small plasma amount from 250 μl to 2 ml plasma. Maximal EVs production have to test or improve in the future. At present, the authors of the present study remain in a small team with limited funding and patient samples and they are testing/planning in different types of cancer by using EXÖBead®.

In the present study, focus was primarily addressed on the isolation of EVs from the blood of cancer patients and their analysis. The focus was primarily on potential diagnostic use. However, the field of therapeutic use of EVs has also grown rapidly in recent years.

One of the advantages is that EVs transport proteins and nucleic acids and protect their contents from proteases and RNAses through their double membrane. They are histocompatible, not recognized by the complement system, do not trigger unwanted immune reactions due to their endogenous origin, and are less rapidly removed by the mononuclear phagocyte system due to their nanoscale size (59) This predisposes

them as carriers for various biological therapeutics, including short interfering RNA (siRNA) and recombinant proteins.

Different techniques are used to cargo EVs with the desired drug load. A distinction is made between exogenous and endogenous loading. The successful use of EVs for targeted delivery of siRNA was first demonstrated in 2011 by Alvarez-Erviti *et al* (60). Herein, isolated EVs were loaded with siRNA against an important protein in Alzheimer's Disease pathogenesis (BACE1) and injected systemically. This resulted in a decrease (55%) of the deleterious protein β-amyloid 1-42 in the brain. Particularly in cancers where target mutations are known, this may be a promising approach. An additional possibility is to overcome chemotherapy resistance by means of EVs. Paclitaxel-loaded EVs have been shown to increase cytotoxicity in multidrug-resistant neoplasms almost 50-fold compared with paclitaxel without EVs (61). A similar approach exists with doxorubicin (62). Particularly for these therapeutic uses, it is considered that is necessary to have a fast and reliable isolation method available that preserves biological activity, as in the case of EXÖBead®. However, it remains to be clarified what effect the loading process has. Although knowledge of EVs has multiplied in recent years, overseeing the complexities remains far. To date, the effects of modifications on their biological behavior cannot be predicted with sufficient reliability. Great potential in EVs is also observed in the field of cancer immunotherapy due to their ability to induce tumor-specific immunity, they are being traded as potential cancer vaccines, with animal and clinical studies already conducted (63). Particularly in this context, it is essential that the biological characteristics of EVs are not altered during the isolation process, hence advantages are observed in the less aggressive elution process using lactose buffer. Nevertheless, it is important to keep in mind that due to the dual properties of EVs (they can both inhibit and promote cancer development), a particularly good comprehension of the underlying mechanisms is required. In summary, the therapeutic use of EVs is a promising one, where the unaltered preservation of biological activity is probably even more important than in the context of diagnostic purposes.

To conclude, the EXÖBead® technique has been shown to provide reliable results in the isolation of EVs in the present study, which proved to be functional. It was possible to perform the isolation with a significantly reduced time (~2 h), since pre-isolation and ultracentrifugation are obsolete here. Hereby, coming from the temporal expenditure into ranges, which make an integration into the clinical routine examination imaginable. Basic requirements for clinical use, such as reliability, time efficiency and manageable costs, are fulfilled as far as manageable to date. In addition to continuous monitoring of cancer development in the clinical setting, the EXÖBead®-based isolation technique can also provide a valuable simplification of sample preparation for research purposes to understand the role of EVs in cancer in an improved way.

Acknowledgements

The authors would like to thank the imaging facility of the department of biomedicine University Basel, particularly Carola Alampi and Mohamed Chami for acquiring the TEM images.

Funding

The present study was supported by the 'pro patient' grant (grant no. pp18-08) and Krebsliga 462 beider Basel (grant no. 18-463 2016).

Availability of data and materials

The datasets used and/or analyzed in the current study are available to us in their complete form and are available upon request from the corresponding author.

Authors' contributions

LB, EE, DMC, MWP and LM conceptualized the present study. DMC, LB and EE curated data. DMC, LB, and LM performed formal analysis. LM acquired funding. Investigation Methodology: DMC, LB, EE, MWP and LM provided investigation methodology. LM performed project administration. LM, DMC and MWP provided resources. DMC, LB and LM performed software analysis. LM and MWP supervised the study. LB, DMC, MWP and LM conducted data validation. LB, DMC and LM performed visualization. LB and EE wrote the original manuscript. LB and DMC revised and finalized the manuscript. LM provided supervision, reviewed and edited the finalized manuscript. MWP reviewed and edited the finalized manuscript. All authors have read and approved the final version of the manuscript.

Ethics approval and consent to participate

The present study was approved (approval no. 2020-02173) by the ethical commission of the northwest and central Switzerland. All patients provided written informed consent for research and consented to anonymous processing of the blood samples collected for scientific purposes.

Patient consent for publication

Not applicable.

Competing interests

DC is the founder of Biovesicle, Inc. All experiments were conducted without financial contribution, simply scientific advices were obtained. LM and MWP are scientific advisor of Biovesicle, Inc. and did not receive profit.

References

1. Raposo G, Nijman HW, Stoorvogel W, Liejendekker R, Harding CV, Melief CJ and Geuze HJ: B lymphocytes secrete antigen-presenting vesicles. J Exp Med 183: 1161-1172, 1996.
2. Harding C, Heuser J and Stahl P: Receptor-mediated endocytosis of transferrin and recycling of the transferrin receptor in rat reticulocytes. J Cell Biol 97: 329-339, 1983.
3. Lopatina T, Favaro E, Danilova L, Fertig EJ, Favorov AV, Kagohara LT, Martone T, Bussolati B, Romagnoli R, Albera R, *et al*: Extracellular vesicles released by tumor endothelial cells spread immunosuppressive and transforming signals through various recipient cells. Front Cell Dev Biol 8: 698, 2020.
4. Xiao C, Song F, Zheng YL, Lv J, Wang QF and Xu N: Exosomes in head and neck squamous cell carcinoma. Front Oncol 9: 894, 2019.

5. Bray F, Ferlay J, Soerjomataram I, Siegel RL, Torre LA and Jemal A: Global cancer statistics 2018: GLOBOCAN estimates of incidence and mortality worldwide for 36 cancers in 185 countries. CA Cancer J Clin 68: 394-424, 2018.
6. Argiris A, Karamouzis MV, Raben D and Ferris RL: Head and neck cancer. Lancet 371: 1695-1709, 2008.
7. Muller L, Hong CS, Stolz DB, Watkins SC and Whiteside TL: Isolation of biologically-active exosomes from human plasma. J Immunol Methods 411: 55-65, 2014.
8. Theodoraki MN, Hoffmann TK, Jackson EK and Whiteside TL: Exosomes in HNSCC plasma as surrogate markers of tumour progression and immune competence. Clin Exp Immunol 194: 67-78, 2018.
9. Ludwig S, Floros T, Theodoraki MN, Hong CS, Jackson EK, Lang S and Whiteside TL: Suppression of lymphocyte functions by plasma exosomes correlates with disease activity in patients with head and neck cancer. Clin Cancer Res 23: 4843-4854, 2017.
10. Hong CS, Funk S, Muller L, Boyiadzis M and Whiteside TL: Isolation of biologically active and morphologically intact exosomes from plasma of patients with cancer. J Extracell Vesicles 5: 29289, 2016.
11. Beccard IJ, Hofmann L, Schroeder JC, Ludwig S, Laban S, Brunner C, Lotfi R, Hoffmann TK, Jackson EK, Schuler PJ and Theodoraki MN: Immune suppressive effects of plasma-derived exosome populations in head and neck cancer. Cancers (Basel) 12: 1997, 2020.
12. Thery C, Amigorena S, Raposo G and Clayton A: Isolation and characterization of exosomes from cell culture supernatants and biological fluids. Curr Protoc Cell Biol Chapter 3: Unit 3.22, 2006.
13. Bianco NR, Kim SH, Morelli AE and Robbins PD: Modulation of the immune response using dendritic cell-derived exosomes. Methods Mol Biol 380: 443-455, 2007.
14. Theodoraki MN, Yerneni SS, Brunner C, Theodorakis J, Hoffmann TK and Whiteside TL: Plasma-derived exosomes reverse epithelial-to-mesenchymal transition after photodynamic therapy of patients with head and neck cancer. Oncoscience 5: 75-87, 2018.
15. Chen SJ, Tsui PF, Chuang YP, Chiang DML, Chen LW, Liu ST, Lin FY, Huang SM, Lin SH, Wu WL, *et al*: Carvedilol ameliorates experimental atherosclerosis by regulating cholesterol efflux and exosome functions. Int J Mol Sci 20: 5202, 2019.
16. Brierley J, Gospodarowicz MK and Wittekind C: TNM classification of malignant tumours. John Wiley & Sons, Inc., Chichester, West Sussex, UK ; Hoboken, NJ, 2017.
17. Gomes J, Gomes-Alves P, Carvalho SB, Peixoto C, Alves PM, Altevogt P and Costa J: Extracellular vesicles from ovarian carcinoma cells display specific glycosignatures. Biomolecules 5: 1741-1761, 2015.
18. Capello M, Vykoukal JV, Katayama H, Bantis LE, Wang H, Kundnani DL, Aguilar-Bonavides C, Aguilar M, Tripathi SC, Dhillon DS, *et al*: Exosomes harbor B cell targets in pancreatic adenocarcinoma and exert decoy function against complement-mediated cytotoxicity. Nat Commun 10: 254, 2019.
19. Kugeratski FG, Hodge K, Lilla S, McAndrews KM, Zhou X, Hwang RF, Zanivan S and Kalluri R: Quantitative proteomics identifies the core proteome of exosomes with syntenin-1 as the highest abundant protein and a putative universal biomarker. Nat Cell Biol 23: 631-641, 2021.
20. Bachurski D, Schuldner M, Nguyen PH, Malz A, Reiners KS, Grenzi PC, Babatz F, Schauss AC, Hansen HP, Hallek M and von Strandmann EP: Extracellular vesicle measurements with nanoparticle tracking analysis-An accuracy and repeatability comparison between NanoSight NS300 and ZetaView. J Extracell Vesicles 8: 1596016, 2019.
21. Muller L, Mitsuhashi M, Simms P, Gooding WE and Whiteside TL: Tumor-derived exosomes regulate expression of immune function-related genes in human T cell subsets. Sci Rep 6: 20254, 2016.
22. Muller L, Simms P, Hong CS, Nishimura MI, Jackson EK, Watkins SC and Whiteside TL: Human tumor-derived exosomes (TEX) regulate Treg functions via cell surface signaling rather than uptake mechanisms. Oncoimmunology 6: e1261243, 2017.
23. Thery C, Witwer KW, Aikawa E, Alcaraz MJ, Anderson JD, Andriantsitohaina R, Antoniou A, Arab T, Arche F, Atkin-Smith GK, *et al*: Minimal information for studies of extracellular vesicles 2018 (MISEV2018): A position statement of the international society for extracellular vesicles and update of the MISEV2014 guidelines. J Extracell Vesicles 7: 1535750, 2018.
24. Theodoraki MN, Yerneni SS, Hoffmann TK, Gooding WE and Whiteside TL: Clinical significance of PD-L1(+) exosomes in plasma of head and neck cancer patients. Clin Cancer Res 24: 896-905, 2018.
25. Karimi N, Cvjetkovic A, Jang SC, Crescitelli R, Feizi MAH, Nieuwland R, Lötvall J and Lässer C: Detailed analysis of the plasma extracellular vesicle proteome after separation from lipoproteins. Cell Mol Life Sci 75: 2873-2886, 2018.
26. Teng Y, Gao L, Loveless R, Rodrigo JP, Strojan P, Willems SM, Nathan CA, Mäkitie AA, Saba NF and Ferlito A: The hidden link of exosomes to head and neck cancer. Cancers (Basel) 13: 5802, 2021.
27. Whiteside TL: Immune modulation of T-cell and NK (natural killer) cell activities by TEXs (tumour-derived exosomes). Biochem Soc Trans 41: 245-251, 2013.
28. Wieckowski EU, Visus C, Szajnik M, Szczepanski MJ, Storkus WJ and Whiteside TL: Tumor-derived microvesicles promote regulatory T cell expansion and induce apoptosis in tumor-reactive activated CD8+ T lymphocytes. J Immunol 183: 3720-3730, 2009.
29. Canavan JB, Afzali B, Scotta C, Fazekasova H, Edozie FC, Macdonald TT, Hernandez-Fuentes MP, Lombardi G and Lord GM: A rapid diagnostic test for human regulatory T-cell function to enable regulatory T-cell therapy. Blood 119: e57-e66, 2012.
30. Ruitenberg JJ, Boyce C, Hingorani R, Putnam A and Ghanekar SA: Rapid assessment of in vitro expanded human regulatory T cell function. J Immunol Methods 372: 95-106, 2011.
31. Ebnoether E and Muller L: Diagnostic and therapeutic applications of exosomes in cancer with a special focus on head and neck squamous cell carcinoma (HNSCC). Int J Mol Sci 21: 4344, 2020.
32. Liu FT and Rabinovich GA: Galectins as modulators of tumour progression. Nat Rev Cancer 5: 29-41, 2005.
33. Krishnamoorthy L, Bess JW Jr, Preston AB, Nagashima K and Mahal LK: HIV-1 and microvesicles from T cells share a common glycome, arguing for a common origin. Nat Chem Biol 5: 244-250, 2009.
34. Williams C, Royo F, Aizpurua-Olaizola O, Pazos R, Boons GJ, Reichardt NC and Falcon-Perez JM: Glycosylation of extracellular vesicles: Current knowledge, tools and clinical perspectives. J Extracell Vesicles 7: 1442985, 2018.
35. Chen G, Huang AC, Zhang W, Zhang G, Wu M, Xu W, Yu Z, Yang J, Wang B, Sun H, *et al*: Exosomal PD-L1 contributes to immunosuppression and is associated with anti-PD-1 response. Nature 560: 382-386, 2018.
36. Sodar BW, Kittel A, Pálóczi K, Vukman KV, Osteikoetxea X, Szabó-Taylor K, Németh A, Sperlágh B, Baranyai T, Giricz Z, *et al*: Low-density lipoprotein mimics blood plasma-derived exosomes and microvesicles during isolation and detection. Sci Rep 6: 24316, 2016.
37. Otahal A, Kuten-Pella O, Kramer K, Neubauer M, Lacza Z, Nehrer S and Luna AD: Functional repertoire of EV-associated miRNA profiles after lipoprotein depletion via ultracentrifugation and size exclusion chromatography from autologous blood products. Sci Rep 11: 5823, 2021.
38. Zhang X, Borg EGF, Liaci AM, Vos HR and Stoorvogel W: A novel three step protocol to isolate extracellular vesicles from plasma or cell culture medium with both high yield and purity. J Extracell Vesicles 9: 1791450, 2020.
39. van Niel G, Bergam P, Di Cicco A, Hurbain I, Cicero AL, Dingli F, Palmulli R, Fort C, Potier MC, Schurgers LJ, *et al*: Apolipoprotein E regulates amyloid formation within endosomes of pigment cells. Cell Rep 13: 43-51, 2015.
40. Li C, Jiang P, Wei S, Xu X and Wang J: Regulatory T cells in tumor microenvironment: New mechanisms, potential therapeutic strategies and future prospects. Mol Cancer 19: 116, 2020.
41. Yan W and Jiang S: Immune cell-derived exosomes in the cancer-immunity cycle. Trends Cancer 6: 506-517, 2020.
42. Li I and Nabet BY: Exosomes in the tumor microenvironment as mediators of cancer therapy resistance. Mol Cancer 18: 32, 2019.
43. Yang C and Robbins PD: The roles of tumor-derived exosomes in cancer pathogenesis. Clin Dev Immunol 2011: 842849, 2011.
44. Paijens ST, Vledder A, de Bruyn M and Nijman HW: Tumor-infiltrating lymphocytes in the immunotherapy era. Cell Mol Immunol 18: 842-859, 2021.
45. Spector ME, Bellile E, Amlani L, Zarins K, Smith J, Brenner JC, Rozek L, Nguyen A, Thomas D, McHugh JB, *et al*: Prognostic value of tumor-infiltrating lymphocytes in head and neck squamous cell carcinoma. JAMA Otolaryngol Head Neck Surg 145: 1012-1019, 2019.

46. Peltanova B, Raudenska M and Masarik M: Effect of tumor microenvironment on pathogenesis of the head and neck squamous cell carcinoma: A systematic review. Mol Cancer 18: 63, 2019.
47. Uppaluri R, Dunn GP and Lewis JS Jr: Focus on TILs: Prognostic significance of tumor infiltrating lymphocytes in head and neck cancers. Cancer Immun 8: 16, 2008.
48. Andratschke M, Hagedorn H and Nerlich A: Expression of the epithelial cell adhesion molecule and cytokeratin 8 in head and neck squamous cell cancer: A comparative study. Anticancer Res 35: 3953-3960, 2015.
49. Rajjoub S, Basha SR, Einhorn E, Cohen MC, Marvel DM and Sewell DA: Prognostic significance of tumor-infiltrating lymphocytes in oropharyngeal cancer. Ear Nose Throat J 86: 506-511, 2007.
50. Badoual C, Hans S, Rodriguez J, Peyrard S, Klein C, Agueznay NEH, Mosseri V, Laccourreye O, Bruneval P, Fridman WH, *et al*: Prognostic value of tumor-infiltrating CD4+ T-cell subpopulations in head and neck cancers. Clin Cancer Res 12: 465-472, 2006.
51. Hofmann L, Ludwig S, Vahl JM, Brunner C, Hoffmann TK and Theodoraki MN: The emerging role of exosomes in diagnosis, prognosis, and therapy in head and neck cancer. Int J Mol Sci 21: 4072, 2020.
52. Economopoulou P, de Bree R, Kotsantis I and Psyrri A: Diagnostic tumor markers in head and neck squamous cell carcinoma (HNSCC) in the clinical setting. Front Oncol 9: 827, 2019.
53. Dahiya K and Dhankhar R: Updated overview of current biomarkers in head and neck carcinoma. World J Methodol 6: 77-86, 2016.
54. Daassi D, Mahoney KM and Freeman GJ: The importance of exosomal PDL1 in tumour immune evasion. Nat Rev Immunol 20: 209-215, 2020.
55. Schneider S, Kadletz L, Wiebringhaus R, Kenner L, Selzer E, Füreder T, Rajky O, Berghoff AS, Preusser M and Heiduschka G: PD-1 and PD-L1 expression in HNSCC primary cancer and related lymph node metastasis-impact on clinical outcome. Histopathology 73: 573-584, 2018.
56. Johnson DE, Burtness B, Leemans CR, Lui VWY, Bauman JE and Grandis JR: Head and neck squamous cell carcinoma. Nat Rev Dis Primers 6: 92, 2020.
57. Burtness B, Harrington KJ, Greil R, Soulières D, Tahara M, de Castro G Jr, Psyrri A, Basté N, Neupane P, Bratland A, *et al*: Pembrolizumab alone or with chemotherapy versus cetuximab with chemotherapy for recurrent or metastatic squamous cell carcinoma of the head and neck (KEYNOTE-048): A randomised, open-label, phase 3 study. Lancet 394: 1915-1928, 2019.
58. Theodoraki MN, Matsumoto A, Beccard I, Hoffmann TK and Whiteside TL: CD44v3 protein-carrying tumor-derived exosomes in HNSCC patients' plasma as potential noninvasive biomarkers of disease activity. Oncoimmunology 9: 1747732, 2020.
59. Kooijmans SA, Vader P, van Dommelen SM, van Solinge WW and Schiffelers RM: Exosome mimetics: A novel class of drug delivery systems. Int J Nanomedicine 7: 1525-1541, 2012.
60. Alvarez-Erviti L, Seow Y, Yin H, Betts C, Lakhal S and Wood MJ: Delivery of siRNA to the mouse brain by systemic injection of targeted exosomes. Nat Biotechnol 29: 341-345, 2011.
61. Kim MS, Haney MJ, Zhao Y, Mahajan V, Deygen I, Klyachko NL, Inskoe E, Piroyan A, Sokolsky M, Okolie O, *et al*: Development of exosome-encapsulated paclitaxel to overcome MDR in cancer cells. Nanomedicine 12: 655-664, 2016.
62. Tian Y, Li S, Song J, Ji T, Zhu M, Anderson GJ, Wei J and Nie G: A doxorubicin delivery platform using engineered natural membrane vesicle exosomes for targeted tumor therapy. Biomaterials 35: 2383-2390, 2014.
63. Scholl JN, de Fraga Dias A, Pizzato PR, Lopes DV, Moritz CEJ, Jandrey EHF, Souto GD, Colombo M, Rohden F, Sévigny J, *et al*: Characterization and antiproliferative activity of glioma-derived extracellular vesicles. Nanomedicine (Lond) 15: 1001-1018, 2020.